2021 International Conference on Unmanned Aircraft Systems (ICUAS)
Athens, Greece. June 15-18, 2021

Ring Formation Maneuvering with Double Integrator Dynamics*

Dzung Tran†, David Casbeer†, Eloy Garcia†, Isaac E. Weintraub†, and Dejan Milutinović§

***Abstract*— Conventional leader-follower formations restrict the follower to a single desired position relative to the leader. To give the follower more flexibility in motion and to replicate typical human pilot operations, in this paper we propose a control architecture allowing the follower to converge to a ring, which is a set of desired points, relative to the leader. The follower is considered subject to a point-mass aircraft model, which can be transformed into the double integrator kinematics. For that reason, the nonlinear backstepping method is first utilized to design the controller for the double integrator kinematics with input saturation constraints being taken into account. The controller is then converted into control variables for the point-mass model. The stability of the proposed architecture is analyzed. Finally, a numerical example is presented to illustrate the efficacy of the proposed controller.**

I. INTRODUCTION

Formation control has a large number of applications in both civilian and military operations ranging from environmental monitoring, search and rescue missions, security patrol to aerial refueling, to name but a few examples (see, for example, [1]–[7] and references therein). Earlier leader-wingman formations with nonlinear dynamics are studied in [8]–[10]. Since then, various directions have been explored on formation control problems. For example, several optimization techniques have been utilized for estimating the "sweet-spot", where the induced drag is minimum, then the controllers are designed for the follower to reach this desired point [8]–[10]. Other interesting techniques include using a neural network to find the induced wake generated by the leader for estimating the optimal relative position for the follower [11], or utilizing the line-of-sight angles to nearby vehicles for maintaining the desired position in the formation [12]. In recent years, design and analysis by means of graph theory has become a popular tool for developing distributed algorithms allowing for scalable multiagent formations (see, for example, [7], [13]–[18] and references therein). Yet, all aforementioned results only consider a single desired point for the follower relative to the leader in the formation, which confines the follower's movement and sometimes leads to infeasible follower trajectories [19], [20].

In this paper, we propose a control architecture for a formation in which the follower converges to a ring (i.e., a set of desired points) relative to the leader. Specifically, the follower is considered subject to a point-mass aircraft model, which can be transformed into the double integrator kinematics (see, for example, [21]–[23] and references therein). For that reason, the controller is first designed based on the nonlinear backstepping method [24], [25] for the double integrator kinematics with input saturation constraints being taken into account. The controller is then converted into control variables for the point-mass model. The stability of the proposed architecture is theoretically analyzed and discussed in detail. We note that a preliminary result on ring formation maneuvering is first investigated in [26], where single-integrator kinematics are considered. This paper considerably expands the results of [26] by considering the double-integrator kinematics with input saturation constraints.

The organization of this paper is as follows. In Section II, we present the problem formulation. In Section III, the control architecture is proposed along with the stability analysis. An illustrative numerical example is provided in Section IV to illustrate the efficacy of the proposed control architecture. Finally, concluding remarks are summarized in Section V.

Notations. The following notations are adopted throughout this paper: $\mathbb{R}$, $\mathbb{R}^n$, and $\mathbb{R}^{n\times m}$ respectively denote the set of real numbers, $n\times 1$ real column vectors, and $n\times m$ real matrices. We write $(\cdot)^{\mathrm{T}}$ for transpose of a vector or of a matrix, $(\cdot)^{-1}$ for the inverse of a nonsingular matrix, $\|\cdot\|_2$ for the Euclidean norm of a vector or induced two-norm of a matrix. A position or velocity vector without a superscript (e.g., p_f or v_f) indicates the vector is defined in the inertial frame; a position or velocity vector with a superscript (e.g., p_f^A or v_f^A) indicates the vector is defined in the reference frame A. Furthermore, a rotation matrix $\mathcal{R}_A^B$ denotes a transformation from the reference frame A to the reference frame B.

II. PROBLEM FORMULATION

In this paper, we consider a system consisting of two vehicles: a leader and a follower. The leader and the follower are free to move in 3-dimensional Cartesian space. The follower aims to approach any position on a ring of radius R located a distance behind the leader and being parallel to the leader's lateral surface created by y^L and z^L axes as illustrated in Fig. 1. The objective is to design the controller for the follower to reach the ring and stay on it during the mission. For that purpose, we define $p_l \triangleq [p_{lx}, p_{ly}, p_{lz}]^{\mathrm{T}}$ and $p_f \triangleq [p_{fx}, p_{fy}, p_{fz}]^{\mathrm{T}}$ as positions of the leader and the follower in the inertial frame, respectively. In what follows, the point-mass aircraft model is first introduced, then the

†D. Tran, D. Casbeer, E. Garcia, and I. Weintraub are affiliated with the Control Science Center of Excellence at the Air Force Research Laboratory, Wright-Patterson Air Force Base, Ohio 45433, United States of America.

§D. Milutinović is a Professor of the Department of Electrical and Computer Engineering at University of California Santa Cruz, Santa Cruz, CA 95064, United States of America.

*This work has been supported in part by AFOSR LRIR No. 21RQCOR084.

2021 International Conference on Unmanned Aircraft Systems (ICUAS) | 978-1-6654-1535-4/21/$31.00 ©2021 IEEE | DOI: 10.1109/ICUAS51884.2021.9476770

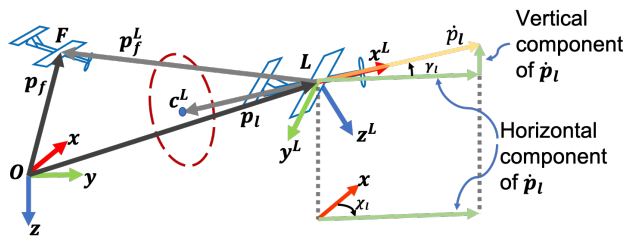

Fig. 1. An illustration of vectors in the inertial frame (black) and the leader body frame (blue) where the leader is located at L, the follower is located at F, and the center of the ring is located at the tip of vector $c^L \in \mathbb{R}^3$.

problem is mathematically stated in the form of the reduced double integrator model.

A. The point-mass aircraft model

We consider the point-mass aircraft model [21] given by

$$\dot{V}_i = \frac{T_i - D_i}{m_i} - g\sin\gamma_i, \tag{1}$$

$$\dot{\gamma}_i = \frac{g}{V_i}(n_i\cos\phi_i - \cos\gamma_i), \tag{2}$$

$$\dot{\chi}_i = \frac{g}{V_i}\frac{n_i\sin\phi_i}{\cos\gamma_i}, \tag{3}$$

$$\dot{p}_{ix} = V_i\cos\gamma_i\cos\chi_i, \tag{4}$$

$$\dot{p}_{iy} = V_i\cos\gamma_i\sin\chi_i, \tag{5}$$

$$\dot{h}_i = V_i\sin\gamma_i, \tag{6}$$

with $i = l$ or $i = f$ being the leader aircraft and the follower aircraft, respectively. In addition, V_i is the ground speed and is assumed to be equal to the air speed, T_i is the thrust, D_i is the aerodynamic drag, m_i is the mass, g is the acceleration due to gravity, γ_i is the flight-path angle, χ is the heading angle, p_{ix} is the downrange, p_{iy} is the crossrange, and $h_i = -p_{iz}$ is the altitude. The load factor n_i, the bank angle ϕ_i and the thrust T_i are the control variable in this model.

By differentiating (4)-(6) with respect to time and substituting the dynamics of V_i, γ_i and ξ_i from (1)-(3), we obtain an alternative model in the form

$$\ddot{p}_{ix} = U_{i1}, \qquad \ddot{p}_{iy} = U_{i2}, \qquad \ddot{h}_i = U_{i3}, \tag{7}$$

where U_{i1}, U_{i2} and U_{i3} are the three new control variables. The relationship between these new variables and the actual variables is given by

$$\phi_i = \arctan\left(\frac{U_{i2}\cos\chi_i - U_{i1}\sin\chi_i}{\cos\gamma_i(U_{i3}+g) - \sin\gamma_i(U_{i1}\cos\chi_i + U_{i2}\sin\chi_i)}\right), \tag{8}$$

$$n_i = \frac{\cos\gamma_i(U_{i3}+g) - \sin\gamma_i(U_{i1}\cos\chi_i + U_{i2}\sin\chi_i)}{g\cos\phi_i}, \tag{9}$$

$$T_i = \big(\sin\gamma_i(U_{i3}+g) + \cos\gamma_i(U_{i1}\cos\chi_i + U_{i2}\sin\chi_i)\big)m_i + D_i. \tag{10}$$

We note that (9) has a singularity at $\phi_i = \frac{\pi}{2}$; however, the maximum bank angle is often limited to below $\frac{\pi}{2}$ in practice. We further assume that D_i is known.

B. Problem Statement

We now consider the follower's dynamics to be given by

$$\dot{p}_f(t) = v_f(t), \tag{11}$$

$$\dot{v}_f(t) = u(t), \tag{12}$$

where $v_f(t) \in \mathbb{R}^3$ is the velocity of the follower and $u(t) \in \mathbb{R}^3$ is the control input. Here, our goal is to design the controller $u(t) = [u_x, u_y, u_z]^{\mathrm{T}}$ subjected to the saturation constraints $\bar{u} \triangleq [\bar{u}_x, \bar{u}_y, \bar{u}_z]^{\mathrm{T}}$ where $\bar{u}_x, \bar{u}_y, \bar{u}_z \in \mathbb{R}_+$ (i.e., $|u_x| \le \bar{u}_x$, $|u_y| \le \bar{u}_y$, $|u_z| \le \bar{u}_z$), so that the follower approaches to the desired ring. We also note that $u_x = U_{f1}$, $u_y = U_{f2}$ and $u_z = -U_{f3}$.

As illustrated in Fig. 1, we have

$$\mathcal{R}_i^L(\gamma,\chi)(p_f(t) - p_l(t)) = \mathcal{R}_i^L(\gamma,\chi)p_d(t) = p_f^L(t), \tag{13}$$

or equivalently,

$$p_f(t) = p_l(t) + \mathcal{R}_L^i(\gamma,\chi)p_f^L(t), \tag{14}$$

where the superscripts and subscripts i and L denote the inertial frame and the leader frame, respectively; $p_d(t) \triangleq p_f(t) - p_l(t)$ denotes the vector $\overrightarrow{LF}$ in the inertial frame, $p_f^L(t)$ is the position of the follower in the leader frame (i.e., the vector $\overrightarrow{LF}$ in the leader frame), and $\mathcal{R}_L^i(\gamma_l,\chi_l)$ is the rotation matrix for the transformation from the leader frame to inertial frame defined by (see, for example, [27, Chapter 2.4])

$$\mathcal{R}_L^i(\gamma_l,\chi_l) \triangleq \begin{bmatrix}\cos(\chi_l) & -\sin(\chi_l) & 0\\ \sin(\chi_l) & \cos(\chi_l) & 0\\ 0 & 0 & 1\end{bmatrix}\begin{bmatrix}\cos(\gamma_l) & 0 & \sin(\gamma_l)\\ 0 & 1 & 0\\ -\sin(\gamma_l) & 0 & \cos(\gamma_l)\end{bmatrix}, \tag{15}$$

with γ_l and χ_l being the leader's flight path angle and course angle, respectively. Fig. 1 also shows how these two angles are defined. In addition, the rotation matrix satisfies the properties $\big(\mathcal{R}_i^L(\gamma_l,\chi_l)\big)^{-1} = \big(\mathcal{R}_i^L(\gamma_l,\chi_l)\big)^{\mathrm{T}} = \mathcal{R}_L^i(\gamma_l,\chi_l)$ and $\det\big(\mathcal{R}_i^L(\gamma_l,\chi_l)\big) = 1$.

Let $c^L \triangleq [c_x^L, c_y^L, c_z^L]^{\mathrm{T}} \in \mathbb{R}^3$ be the center of the ring and $r^{*L} \in \mathbb{R}^3$ be an arbitrary vector in the set of vectors depicting the ring in the leader frame, which is illustrated by the dashed circle in Fig. 1. In other words, the objective is to design the controller $u(t)$ subjected to the aforementioned saturation constraints such that at steady state $p_f(t)$ at least converges to a small neighborhood of $p_l(t) + \mathcal{R}_L^i(\gamma_l,\chi_l)r^{*L}$.

III. RING FORMATION CONTROLLER

In this section, we introduce the procedure to obtain the proposed controller and prove its stability. For that purpose, we first explicitly define the vector r^{*L}. Since the ring surface is parallel to the plane created by y^L and z^L axes, the projection of the follower's position onto ring surface is depicted in Fig. 2. Furthermore, one can define an angle φ based on the follower's position relative to the center of the ring. This angle φ can be used to encode the desired position of the follower on the ring. In other words, the desired position of the follower on the ring at each time moment can be approximated as the intersection of the line from the

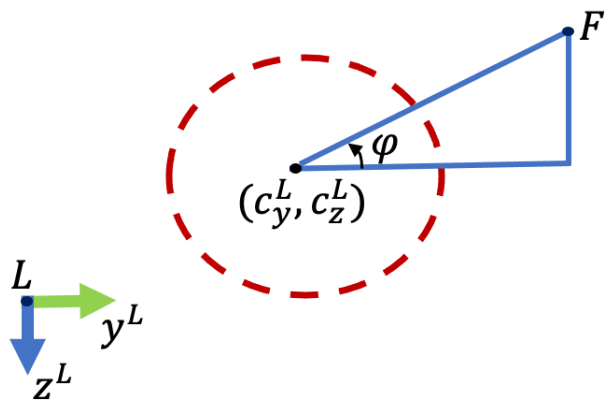

Fig. 2. The projection of the follower's position onto the ring surface with the view from behind toward the leader's tail.

follower to the center and the desired ring. Therefore, we consider

$$r^{*L} \triangleq \begin{bmatrix} c_x^L \\ R\cos(\varphi) + c_y^L \\ R\sin(\varphi) + c_z^L \end{bmatrix}, \tag{16}$$

with R being the radius of the ring and $\varphi(t) \in \mathbb{R}$ obeying

$$\dot{\varphi}(t) = \beta\left(\dot{p}_{fy}^L(t)\sin(\varphi) - \dot{p}_{fz}^L(t)\cos(\varphi)\right), \quad \varphi(0) = \varphi_0, \tag{17}$$

where $\beta \in \mathbb{R}_+$ is a gain, $\dot{p}_{fy}^L(t)$ and $\dot{p}_{fz}^L(t)$ are the second and third components of $\dot{p}_f^L(t)$. The derivation for obtaining the dynamics (17) is discussed in the Appendix. We are now able to define the error

$$e(t) \triangleq \begin{bmatrix} e_x(t) \\ e_y(t) \\ e_z(t) \end{bmatrix} = p_f(t) - p_l(t) - \mathcal{R}_L^i(\gamma_l, \chi_l) r^{*L} \in \mathbb{R}^3. \tag{18}$$

Next, taking the time derivative twice, one obtains

$$\begin{aligned} \ddot{e}(t) &= \ddot{p}_f(t) \underbrace{-\ddot{p}_l(t) - \frac{\mathrm{d}^2 \mathcal{R}_L^i(\gamma_l, \chi_l) r^{*L}}{\mathrm{d}t^2}}_{d(t)} \\ &= u(t) + d(t). \end{aligned} \tag{19}$$

Here, we assume that the position of the leader $p_l(t)$, the leader's flight path angle γ_l and the course angle χ_l are available through information exchange, hence the terms $p_l(t)$ and $\mathcal{R}_L^i(\gamma_l, \chi_l) r^{*L}$ can be constructed and passed through command filters (see, for example, [28], [29]) to obtain their derivatives[1]. As a result, given the observable variables, the term $d(t)$ can be closely approximated as $\hat{d}(t)$.

[1]These derivatives can be directly derived if all necessary information is available. However, the analytic derivation of these derivatives is cumbersome. Therefore, using command filters can simplify the calculation process and they require less information as well. We refer the interested readers to Figure 2 and Appendix A of [28] for the detailed structure of a command filter.

By defining $x_1(t) \triangleq e(t) \in \mathbb{R}^3$ and $x_2(t) \triangleq \dot{e}(t) \in \mathbb{R}^3$, we can write the error dynamics (19) as

$$\dot{x}_1(t) = x_2(t), \tag{20}$$

$$\dot{x}_2(t) = u(t) + d(t), \quad x_1(0) = x_{10}, \; x_2(0) = x_{20}, \tag{21}$$

At this point, the problem is translated into design the controller $u(t) = [u_x, u_y, u_z]^{\mathrm{T}}$ subjected to the saturation constraints such that $x \triangleq [x_1^{\mathrm{T}}, x_2^{\mathrm{T}}]^{\mathrm{T}}$ approaches 0 as $t \to \infty$. In what follows, we utilize the backstepping method to design the controller with saturation constraint.

We start with the Lyapunov function candidate $V_1(x_1) = \frac{1}{2}x_1^{\mathrm{T}}x_1$ and take its time derivative along the trajectory (20) yielding

$$\dot{V}_1 = x_1^{\mathrm{T}}(t)x_2(t). \tag{22}$$

Treating $x_2(t)$ as the control input, one can choose $x_2(t) = -k_1 x_1(t)$ with $k_1 \in \mathbb{R}_+$ to make the origin of $\dot{x}_1(t) = -k_1 x_1(t)$ globally asymptotically stable. To backstep, we define a new variable

$$s(t) \triangleq x_2(t) + k_1 x_1(t) + \xi(t), \tag{23}$$

where $\xi(t) \in \mathbb{R}^3$ is an extra term to compensate for the input saturation. In addition, $\xi(t)$ satisfies

$$\dot{\xi}(t) = -k_2\xi(t) + \Delta u(t), \quad \xi(0) = \xi_0, \tag{24}$$

where $k_2 \in \mathbb{R}_+$ is a constant gain, $\Delta u(t) \triangleq u_d(t) - u_a(t)$ with $u_d(t) \triangleq [u_{dx}, \; u_{dy}, \; u_{dz}]^{\mathrm{T}}$ being the designed controller and $u_a(t)$ being the saturated controller defined by

$$u_a(t) \equiv u(t) \triangleq \mathrm{sat}(u_d) = [\mathrm{sat}(u_{dx}), \; \mathrm{sat}(u_{dy}), \; \mathrm{sat}(u_{dz})]^{\mathrm{T}}. \tag{25}$$

Note that $\mathrm{sat}(u_{di}) = \mathrm{sign}(u_{di})\min\{|u_{di}|, \bar{u}_i\}$ for $i = x, y, z$. Utilizing (23), the expression (22) can be rewritten as

$$\dot{V}_1 = x_1^{\mathrm{T}}(t)\left(s(t) - k_1 x_1(t) - \xi(t)\right). \tag{26}$$

Furthermore, taking time derivative of (23) and substituting (20), (21), and (24) into (23) yields

$$\begin{aligned} \dot{s}(t) &= u(t) + d(t) + k_1 x_2(t) - k_2\xi(t) + \Delta u(t) \\ &= d(t) + k_1 x_2(t) - k_2\xi(t) + u_d(t), \end{aligned} \tag{27}$$

where the second equality comes from the definition of $\Delta u(t)$.

Consider the Lyapunov function candidate

$$\begin{aligned} V_2(x_1, s) &= V_1(x_1) + \frac{1}{2}s^{\mathrm{T}}s \\ &= \frac{1}{2}x_1^{\mathrm{T}}x_1 + \frac{1}{2}s^{\mathrm{T}}s, \end{aligned} \tag{28}$$

where $V_2(0,0) = 0$ and $V_2(x_1, s) > 0$ for all $(x_1, s) \neq 0$. Taking the time derivative of (28) along the trajectories of (26) and (27), we have

$$\begin{aligned} \dot{V}_2 =& x_1^{\mathrm{T}}(t)x_2(t) + s^{\mathrm{T}}\dot{s} \\ =& x_1^{\mathrm{T}}(t)\left(s(t) - k_1 x_1(t) - \xi(t)\right) \\ &+ s^{\mathrm{T}}\left(d(t) + k_1 x_2(t) - k_2\xi(t) + u_d(t)\right) \\ =& -k_1 x_1^{\mathrm{T}}(t)x_1(t) + x_1^{\mathrm{T}}(t)\left(s(t) - \xi(t)\right) \\ &+ s^{\mathrm{T}}\left(d(t) + k_1 x_2(t) - k_2\xi(t) + u_d(t)\right), \end{aligned} \tag{29}$$

By choosing the controller

$$u_d(t) = -\hat{d}(t) - k_1 x_2(t) + k_2 \xi(t) - k_3 s(t) - x_1(t), \quad (30)$$

where $k_3 \in \mathbb{R}_+$ is a constant gain and $\hat{d}(t)$ is the approximation of $d(t)$ obtained through the command filters. As a result, (29) becomes

$$\dot{V}_2 = -k_1 x_1^{\mathrm{T}}(t) x_1(t) - k_3 s^{\mathrm{T}}(t) s(t) - x_1^{\mathrm{T}}(t)\xi(t) + s^{\mathrm{T}} \Delta d(t), \quad (31)$$

where $\Delta d(t) \triangleq d(t) - \hat{d}(t)$.

We now recap the result of this section with the following theorem.

Theorem 1. *Consider the double integrator dynamics of the follower in the leader frame given by (11)-(12) and the reference vector r^{L*} defined by (16)-(17), if the follower executes the controller $u_a(t)$ given by (25) where $u_d(t)$ are given in (30) and $s(t)$ and $\xi(t)$ are designed according to (23)-(24), then the origin of the closed-loop error dynamics given by (20), (21) and (27) is input-to-state stable with $\xi(t)$ and $\Delta d(t)$ being considered as the inputs.*

Proof. One can easily verify that when $\xi(t) = 0$ and $\Delta d(t) = 0$, then $u_d(t) = u_a(t) = u(t)$ and the origin of the closed-loop error dynamics given by (20), (21) and (27) is exponentially stable. With the Lyapunov function (28) and $0 < \theta_1 < k_1$ and $0 < \theta_2 < k_3$, the time derivative (31) can be rewritten as

$$\begin{aligned}\dot{V}_2 =& -(k_1 - \theta_1) x_1^{\mathrm{T}}(t) x_1(t) - (k_3 - \theta_2) s^{\mathrm{T}}(t) s(t) \\ & - \theta_1 x_1^{\mathrm{T}}(t) x_1(t) - x_1^{\mathrm{T}}(t)\xi(t) - \theta_2 s^{\mathrm{T}}(t) s(t) + s^{\mathrm{T}} \Delta d(t) \\ \leq& -(k_1 - \theta_1) x_1^{\mathrm{T}}(t) x_1(t) - (k_3 - \theta_2) s^{\mathrm{T}}(t) s(t), \\ & \forall\ (x_1, s) \in \mathcal{S}. \quad (32)\end{aligned}$$

where

$$\mathcal{S} \triangleq \left\{ (x_1, s) : \|x_1(t)\|_2 \geq \frac{\|\xi(t)\|_2}{\theta_1}, \|s(t)\|_2 \geq \frac{\|\Delta d(t)\|_2}{\theta_2} \right\}. \quad (33)$$

Thus, by [25, Lemma 4.5], the system is input-to-state stable. ■

Remark 1. *If the term $d(t)$ can be accurately approximated through command filters, then $\Delta d(t) = 0$. In addition, if no input saturation occurs after finite time, that is, there exists a finite time $\tau \in \mathbb{R}_+$ such that $\Delta u(t) = 0$ for $t \geq \tau$. As a result, the dynamics (24) indicates the compensative term $\xi(t)$ exponentially converges to 0 for $t > \tau$. From the proof of Theorem 1, we can conclude that when $\xi(t)$ converges to zero, so does $x_1(t)$ and $s(t)$. Since $x_2(t) = s(t) - k_1 x_1(t) - \xi(t)$, when $x_1(t)$, $s(t)$, and $\xi(t)$ approach 0 as $t \to \infty$, so does $x_2(t)$. In other words, if the term $d(t)$ can be perfectly approximated and the input saturation vanishes after finite time, the error asymptotically converges to zero.*

Remark 2. *If the terms $\Delta d(t)$ and $\xi(t)$ are persistent and bounded such that $\|\Delta d(t)\|_2 \leq \Delta^*$ and $\|\xi\|_2 \leq \xi^*$,[2] then the solutions of the closed-loop error dynamics given by (20), (21) and (27) are uniformly bounded. Specifically, from (31), we can directly see that $\dot{V}_2(x_1(t), s(t)) < 0$ outside the compact set given by*

$$\Omega \triangleq \left\{ (x_1, s) : \|x_1(t)\|_2 \leq \frac{\xi^*}{k_1}, \|s(t)\|_2 \leq \frac{\Delta^*}{k_3} \right\}. \quad (34)$$

Therefore, there exists some T such that for $t \geq T$, $V_2(x_1(t), s(t))$ defined in (28) is upper bounded by

$$\begin{aligned} V_2(x_1(t), s(t)) \leq & \max_{(x_1(t), s(t)) \in \Omega} V_2(x_1(t), s(t)) \\ = & \frac{1}{2}\left(\left(\frac{\xi^*}{k_1}\right)^2 + \left(\frac{\Delta^*}{k_3}\right)^2 \right), \quad \forall\ t \geq T. \end{aligned} \quad (35)$$

In addition, from (28), we have $\frac{1}{2} x_1^{\mathrm{T}}(t) x_1(t) \leq V_2(x_1(t), s(t))$. As a result, one can obtain the ultimate performance bound of the error $x_1(t)$ for $t \geq T$ as

$$\|x_1(t)\|_2 \leq \sqrt{\left(\frac{\xi^*}{k_1}\right)^2 + \left(\frac{\Delta^*}{k_3}\right)^2}. \quad (36)$$

Remark 3. *We note that the main cause for input saturation is a large initial error, where the follower is far away from the leader, hence the assumption that no input saturation occurs after finite time is a reasonable one. This assumption also indicates that the follower has the capability to catch up with the leader. On the other hand, if the input saturation lasts indefinitely, (24) indicates that $\xi(t)$ will never converge to 0. As a result, even when $x_1(t)$ and $s(t)$ reach 0 according to (31), the definition (23) indicates that $x_2(t) = -\xi(t) \neq 0$; that is, it is impossible for the close-loop error dynamics (19) to reach the origin. Such a scenario is when the follower is much slower compared to the leader, thus not only the input saturation lasts indefinitely but also the follower can not reduce the error over time.*

Remark 4. *The proposed control architecture can also be applied to a single-point relative formation. Specifically, one can choose a specific value for $\varphi(t)$ (i.e., $\dot{\varphi}(t) = 0$ in (17)). As a result, r^{*L} in (16) is a specific desired point.*

Remark 5. In order to implement the proposed control architecture, the follower needs to know the leader's position $p_l(t)$, velocity $\dot{p}_l(t)$ as well as the flight path angle γ_l, the course angle χ_l for constructing $\mathcal{R}_L^i(\gamma_l, \chi_l)$. This can be a challenge if the leader is not a cooperative agent or if the communication is lost during the mission. Fortunately, if the follower knows the leader's position $p_l(t)$ and assume that the sampling time is sufficiently small, all other information can be inferred. More details, the leader's position $p_l(t)$ can be passed through a command filter (see, for example,

[2]Based on (24), ξ^* can be calculated if the upper bound of $\|\Delta u(t)\|_2$ is given. In practice, one can set an upper bounds u^* for $u_d(t)$ (see, for example, [30]), then the upper bound of $\|\Delta u(t)\|_2$ can be calculated from $u^* - \bar{u}$.

[28]) to obtain $\dot{p}_l(t)$, and once again, $\dot{p}_l(t)$ is passed through another command filter to obtain $\ddot{p}_l(t)$. Subsequently, provided that the inertial frame use the North-East-Down (NED) convention, then the flight path angle can be obtained by $\gamma_l = \arctan\left(\frac{-\dot{p}_{lz}}{\sqrt{\dot{p}_{lx}^2+\dot{p}_{ly}^2}}\right)$ and the course angle is given by $\chi_l = \arctan\left(\frac{\dot{p}_{ly}}{\dot{p}_{lx}}\right)$. Another common scenario is that there is no information exchange between the leader and the follower, yet the follower has the ability to measure the range vector between the two vehicles; that is, the position of the leader in the follower frame $p_l^F(t) = \mathcal{R}_i^L(\gamma_f, \chi_f)\left(p_l(t) - p_f(t)\right)$ is given, where γ_f and χ_f are the follower's flight path angle and course angle, respectively. In this case, it is reasonable to assume that the follower knows its position and angles, then the leader position $p_l(t)$ in the inertial frame can be calculated and other information can be inferred as in the aforementioned procedure.

IV. NUMERICAL EXAMPLE

For this numerical example, we consider the leader and the follower are Aerosonde UAVs with $m = 13.5$ kg [27, Appendix E]. The leader's and follower's initial positions are at $[-300; -500; 1000]$ and $[-360; -460; 1050]$, respectively. The desired ring is chosen to have the radius $R = 10$ m and the center is located at $c^L = [-10; 0; 0]$. The leader is commanded to travel at a constant speed of 15 m/s and to track a sinusoidal trajectory on the x-y plane depicted by $\gamma(t) = 0$ and $\chi(t) = 2\cos\left(0.2t - \frac{\pi}{2}\right)$. The follower has an initial speed of 12 m/s. The gain $\beta = 0.5$ is chosen for the update law (17). The control algorithm $u_a(t)$ (25) is implemented with $u_d(t)$ being given by (30) and $\bar{u} = [10\ 10\ 10]^{\mathrm{T}}$. In addition, the constant gains are set to $k_1 = 8.17$, $k_2 = 1$, $k_3 = 0.4896$.

Figures 3-5 depict the performance of the follower. Specifically, Fig. 3 shows the leader's and follower's trajectories during the mission and demonstrates the follower's ability to approach and stay on the desired ring. Fig. 4 shows that the error $e(t)$ defined in (18) quickly converges to a small neighborhood of zero. Furthermore, Fig. 5 shows that $\xi(t)$ and $s(t)$ converge to zeros and the controller satisfies the saturation constraint. Here, we note that the controller is only saturated at the beginning of the mission due to a large initial error. Therefore, the numerical example illustrates the efficacy of the proposed control algorithm.

To further illustrate the the proposed algorithm, the above numerical example is repeated with different initial conditions. In particular, the followers are initially located at $[-360; -460; 1050]$, $[-330; -420; 990]$ and $[-310; -520; 970]$, respectively. Figure 6 illustrates the evolution of the followers under the proposed control algorithm (25). It can be seen that the followers with different initial conditions converge to different positions on the ring.

V. CONCLUSIONS

The paper introduced a controller allowing the follower to converge to a ring, which is a set of desired points, relative to the leader. The procedure to design the controller together with the proof of stability were presented in detail. The numerical example also showed the efficacy of the proposed controller. For future works, we will investigate the distribution of multiple followers on the same ring with collision avoidance among the vehicles and will consider developing a discretized controller for practical implementation.

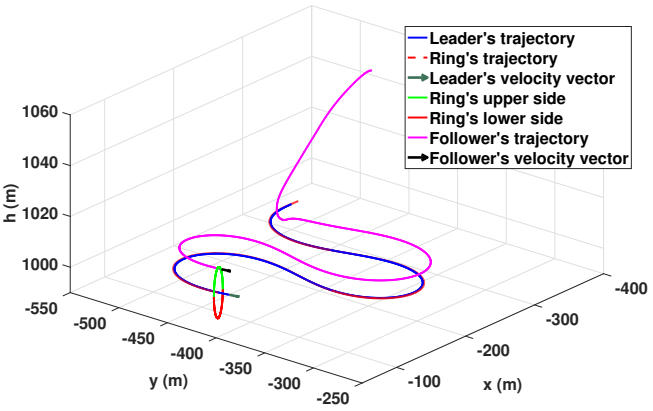

Fig. 3. The evolution of the follower under the proposed algorithm (25).

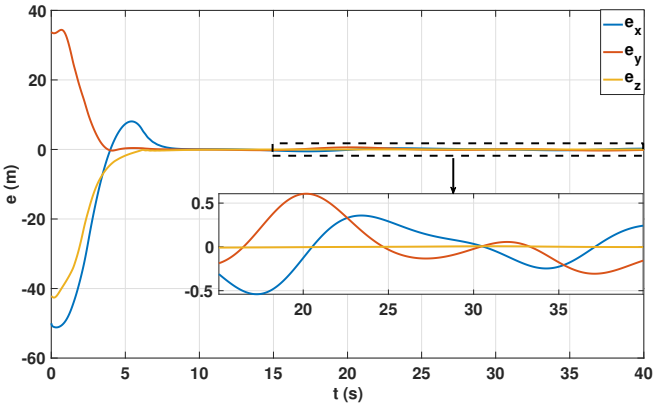

Fig. 4. The evolution of the error $e^L(t)$ defined in (18).

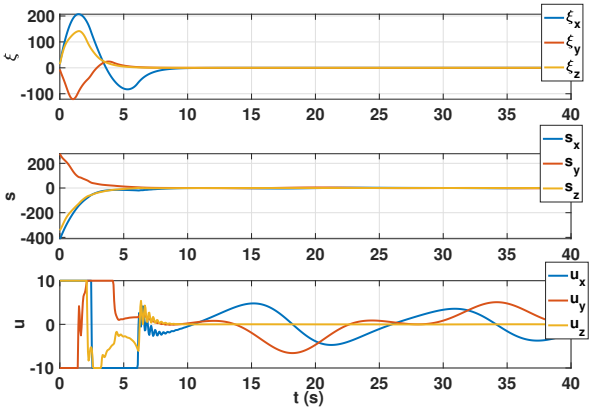

Fig. 5. The evolution of $\xi(t)$ (top), $s(t)$ (middle) and $u(t)$ (bottom).

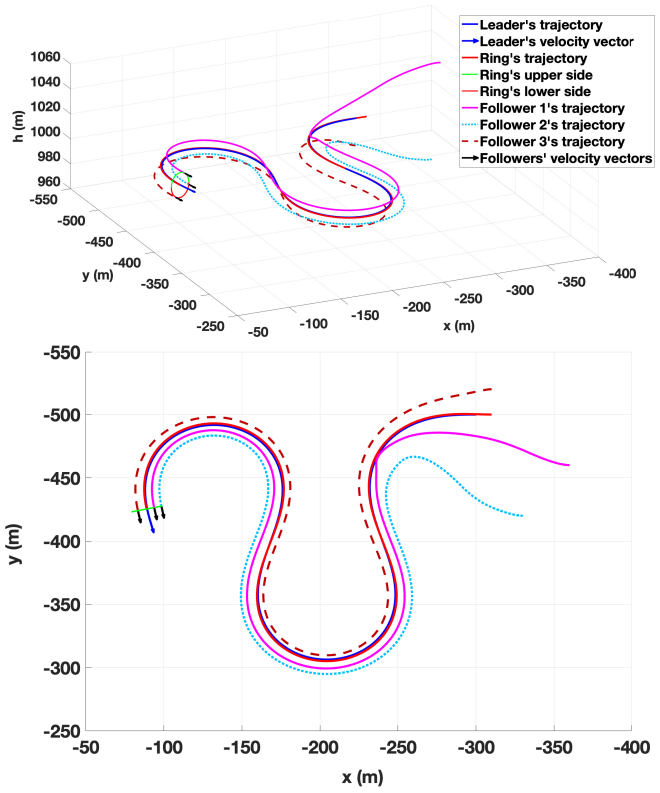

Fig. 6. The evolution of the followers with (Top) side-view and (Bottom) top-view under the proposed algorithm (25).

APPENDIX

In general, one has the freedom to choose an update law for $\varphi(t)$. In fact, the rate of change given by (17) is derived from choosing $\varphi(t) = \arctan\left(\frac{c_z^L - p_{fz}^L}{c_y^L - p_{fy}^L}\right)$ with some modification. To elucidate this point, taking the time derivative of the previous expression yields

$$\begin{aligned}\dot{\varphi}(t) &= \frac{(c_y^L - p_{fy}^L)^2}{(c_y^L - p_{fy}^L)^2 + (c_z^L - p_{fz}^L)^2}\left(\frac{\dot{p}_{fy}^L(c_z^L - p_{fz}^L)}{(c_y^L - p_{fy}^L)^2} - \frac{\dot{p}_{fz}^L}{c_y^L - p_{fy}^L}\right) \\ &= \frac{\dot{p}_{fy}^L(c_z^L - p_{fz}^L) - \dot{p}_{fz}^L(c_y^L - p_{fy}^L)}{(c_y^L - p_{fy}^L)^2 + (c_z^L - p_{fz}^L)^2}. \end{aligned} \tag{37}$$

Let $d \triangleq \sqrt{(c_y^L - p_{fy}^L)^2 + (c_z^L - p_{fz}^L)^2}$. In addition, using the fact that $\sin(\varphi) = \frac{c_z^L - p_{fz}^L}{d}$ and $\cos(\varphi) = \frac{c_y^L - p_{fy}^L}{d}$, (37) can be rewritten as

$$\begin{aligned}\dot{\varphi}(t) &= \frac{1}{d}\left(\frac{\dot{p}_{fy}^L(c_z^L - p_{fz}^L)}{d} - \frac{\dot{p}_{fz}^L(c_y^L - p_{fy}^L)}{d}\right) \\ &= \frac{1}{d}\left(\dot{p}_{fy}^L \sin(\varphi) - \dot{p}_{fz}^L \cos(\varphi)\right). \end{aligned} \tag{38}$$

To avoid singularity, the coefficient $\frac{1}{d}$ in (38) is replaced by a positive constant gain β in (17). If a big value is chosen for the gain β, ϕ quickly reacts to any change in positions of both the leader and the follower leading to possible undesired oscillations. On the other hand, if the gain β is too small, ϕ is insensitive to the change in positions of the vehicles. From the rule of thumb, β is often set to a value that is less than 1.

We further note that in general, when the desired ring surface is not parallel to the surface created by y^L and z^L axes, the angle $\varphi(t)$ can be obtained as follow:

- From the center of the ring, we can define the ring frame to describe its orientation. In particular, we consider that the x^C axes are perpendicular to the ring surface, and the y^C and z^C axes are on the ring surface and perpendicular to each other, where the superscripts C denote the ring frame. As a result, a rotation matrix from the leader frame to the ring frame $\mathcal{R}_L^C(\mu, \beta, \alpha)$ can be constructed, where α-β-μ is the rotation sequence along the z-y-x starting from the Leader frame.
- The position of the follower in the ring frame is given by $p_f^C(t) = [p_{fx}^C, p_{fy}^C, p_{fz}^C]^{\mathrm{T}} = \mathcal{R}_L^C(\mu, \beta, \alpha)(p_f^L - c^L)$.
- The angle $\varphi(t)$ is now defined as $\varphi(t) = \arctan\left(\frac{p_{fz}^C}{p_{fy}^C}\right)$.

After that, one can take the time derivative of $\varphi(t)$ similar to the aforementioned method to obtain the update law for $\varphi(t)$.

REFERENCES

[1] B. Bayat, N. Crasta, A. Crespi, A. M. Pascoal, and A. Ijspeert, "Environmental monitoring using autonomous vehicles: A survey of recent searching techniques," *Current Opinion in Biotechnology*, vol. 45, pp. 76–84, 2017.

[2] M. A. Goodrich, B. S. Morse, D. Gerhardt, J. L. Cooper, M. Quigley, J. A. Adams, and C. Humphrey, "Supporting wilderness search and rescue using a camera-equipped mini uav," *Journal of Field Robotics*, vol. 25, no. 1-2, pp. 89–110, 2008.

[3] A. R. Girard, A. S. Howell, and J. K. Hedrick, "Border patrol and surveillance missions using multiple unmanned air vehicles," in *Conference on Decision and Control*, vol. 1. IEEE, 2004, pp. 620–625.

[4] M. Pachter, C. H. Houpis, and D. Trosen, "Design of an air-to-air automatic refueling flight control system using quantitative feedback theory," *International Journal of Robust and Nonlinear Control*, 1997.

[5] M. D. Tandale, R. Bowers, and J. Valasek, "Trajectory tracking controller for vision-based probe and drogue autonomous aerial refueling," *Journal of Guidance, Control, and Dynamics*, vol. 29, no. 4, pp. 846–857, 7 2006.

[6] S. Ross, M. Pachter, D. Jacques, B. Kish, and D. Millman, "Autonomous aerial refueling based on the tanker reference frame," in *IEEE Aerospace Conference*, vol. 2006, 2006, pp. 1–22.

[7] K.-K. Oh, M.-C. Park, and H.-S. Ahn, "A survey of multi-agent formation control," *Automatica*, vol. 53, pp. 424–440, 3 2015.

[8] L. Buzogany, M. Pachter, and J. D'azzo, "Automated control of aircraft in formation flight," in *Guidance, Navigation and Control Conference*. American Institute of Aeronautics and Astronautics, 8 1993, pp. 1349–1370.

[9] M. Pachter, J. J. D'Azzo, and J. L. Dargan, "Automatic formation flight control," *Journal of Guidance, Control, and Dynamics*, vol. 17, no. 6, pp. 1380–1383, 11 1994.

[10] V. P. Reyna, "Automation of formation flight control," Ph.D. dissertation, Air Force Institute of Technology, 1994.

[11] L. Pollini, M. Innocenti, and F. Giulietti, "Sensorless formation flight," in *AIAA Guidance, Navigation, and Control Conference and Exhibit*, no. August, 8 2001.

[12] M.-J. Tahk, C.-S. Park, and C.-K. Ryoo, "Line-of-sight guidance laws for formation flight," *Journal of Guidance, Control, and Dynamics*, vol. 28, no. 4, pp. 708–716, 7 2005.

[13] M. Mesbahi and M. Egerstedt, *Graph Theoretic Methods in Multiagent Networks*. Princeton University Press, 2010.

[14] F. L. Lewis, H. Zhang, K. Hengster-Movric, and A. Das, *Cooperative Control of Multi-Agent Systems: Optimal and Adaptive Design Approaches*. Springer Science & Business Media, 2013.

[15] D. Tran, T. Yucelen, and E. L. Pasiliao, "Formation control with multiplex information networks," *IEEE Transactions on Control Systems Technology*, vol. 28, no. 2, pp. 462–476, 3 2020.
[16] D. Gu, "A differential game approach to formation control," *IEEE Transactions on Control Systems Technology*, vol. 16, no. 1, pp. 85–93, 2008.
[17] H. Rezaee and F. Abdollahi, "Pursuit formation of double-integrator dynamics using consensus control approach," *IEEE Transactions on Industrial Electronics*, vol. 62, no. 7, pp. 4249–4256, 2015.
[18] Z. Sun, B. D. Anderson, M. Deghat, and H.-S. Ahn, "Rigid formation control of double-integrator systems," *International Journal of Control*, vol. 90, no. 7, pp. 1403–1419, 2017.
[19] S.-J. Kim and I.-H. Whang, "Acceleration constraints for maneuvering formation flight trajectories," *IEEE Transactions on Aerospace and Electronic Systems*, vol. 48, no. 2, pp. 1052–1060, 2012.
[20] D. Milutinović and D. W. Casbeer, "Leader-follower formation feedback control composed of turning rate and velocity controllers," in *2020 International Conference on Unmanned Aircraft Systems*. IEEE, 2020, pp. 1189–1198.
[21] P. Menon, "Short-range nonlinear feedback strategies for aircraft pursuit-evasion," *Journal of Guidance, Control, and Dynamics*, vol. 12, no. 1, pp. 27–32, 1989.
[22] Y. Zou, P. R. Pagilla, and E. Misawa, "Formation of a group of vehicles with full information using constraint forces," *Journal of Dynamic Systems, Measurement, and Control*, vol. 129, no. 5, pp. 654–661, 9 2007.
[23] Y. Zou, P. R. Pagilla, and R. T. Ratliff, "Distributed formation flight control using constraint forces," *Journal of Guidance, Control, and Dynamics*, vol. 32, no. 1, pp. 112–120, 1 2009.
[24] P. V. Kokotovic, "The joy of feedback: Nonlinear and adaptive," *IEEE Control Systems Magazine*, vol. 12, no. 3, pp. 7–17, 1992.
[25] H. K. Khalil, *Nonlinear Control*. Pearson Higher Ed, 2014.
[26] D. M. Tran, D. Casbeer, E. Garcia, I. E. Weintraub, D. Milutinović, and S. G. Manyam, "Ring formation maneuver: Single-integrator kinematics," in *AIAA Scitech 2021 Forum*, 2021, p. 0978.
[27] R. W. Beard and T. W. McLain, *Small Unmanned Aircraft: Theory and Practice*. Princeton university press, 2012.
[28] J. Farrell, M. Sharma, and M. Polycarpou, "Backstepping-based flight control with adaptive function approximation," *Journal of Guidance, Control, and Dynamics*, vol. 28, no. 6, pp. 1089–1102, 2005.
[29] J. A. Farrell, M. Polycarpou, M. Sharma, and W. Dong, "Command filtered backstepping," *IEEE Transactions on Automatic Control*, vol. 54, no. 6, pp. 1391–1395, 2009.
[30] M. Fu, "Linear quadratic control with input saturation," in *Perspectives in Robust Control*. Springer, 2001, pp. 57–67.